JOURNAL OF SPACECRAFT AND ROCKETS
Vol. 40, No. 3, May–June 2003

Pitch Control During Autonomous Aerobraking for Near-Term Mars Exploration

Wyatt R. Johnson* and James M. Longuski†
Purdue University, West Lafayette, Indiana 47907-1282
and
Daniel T. Lyons‡
Jet Propulsion Laboratory, California Institute of Technology, Pasadena, California 91109-8099

Conventional aerobraking requires propellant to dump the spacecraft's angular momentum and to maintain attitude control during the atmospheric flythrough. We consider how reaction wheels can be used to control the spacecraft's pitch during each atmospheric flythrough and to reduce angular momentum simultaneously. Control laws are developed for minimum onboard instrumentation (where the only state information are the angular rates of the spacecraft and the reaction wheels) to compensate for large variations in entry time and atmospheric density. Simulations indicate that pitch attitude and angular momentum can be controlled with reaction wheels alone, thus saving precious propellant while significantly increasing the timing margin for sequencing.

Nomenclature

A = system matrix
A_{ref} = reference area of spacecraft, m^2
B = input matrix or momentum bias
C = output matrix
C_D = coefficient of drag
C_L = coefficient of lift
C_{M_α} = derivative of spacecraft's aerodynamic moment coefficient with respect to angle of attack, deg^{-1}
E = affine term
e = eccentricity
G = momentum gain
g = gravitational acceleration, m/s^2
H = angular momentum, $kg \cdot m^2/s$
I = moment of inertia, $kg \cdot m^2$
$\boldsymbol{K}$ = feedback gain vector
L_{ref} = reference length of spacecraft, m
m = mass of spacecraft, kg
r = radius of spacecraft's orbit, km
u = control input to reaction wheel (commanded torque), $N \cdot m$
V = velocity of spacecraft relative to planet, km/s
$\boldsymbol{x}$ = state vector
α = angle of attack, deg
β = inverse scale height of atmosphere, km^{-1}
γ = flight-path angle, deg
θ = true anomaly, deg
μ = gravitational parameter, km^3/s^2
ρ = atmospheric density, kg/m^3
σ = bank angle, deg
ϕ = latitude, deg
ψ = spacecraft heading, deg
Ω = inertial angular rate of reaction wheel, rad/s
ω = inertial angular rate of spacecraft about pitch axis, rad/s

Subscripts

e = equilibrium
f = postflyby condition
i = preflyby condition
p = periapsis
rw = reaction wheel
sc = spacecraft (not including reaction wheel)
0 = reference value

Presented as Paper AAS 01-388 at the AAS/AIAA Astrodynamics Specialists Conference, Quebec, QC, Canada, 30 July–2 August 2001; received 14 July 2002; revision received 23 October 2002; accepted for publication 12 November 2002.

*Doctoral Candidate, School of Aeronautics and Astronautics; currently Senior Engineer, Navigation and Mission Design, Jet Propulsion Laboratory, California Institute of Technology, 4800 Oak Grove Drive, Pasadena, CA, 91109. Student Member AIAA.

†Professor, School of Aeronautics and Astronautics. Associate Fellow AIAA.

‡Senior Engineer, Navigation and Mission Design, 4800 Oak Grove Drive.

Introduction

PROPELLANT is a cost driver in launching and delivering an interplanetary spacecraft to its final destination, but upon arrival expenditure of additional propellant to insert the spacecraft into orbit is wasteful if there are alternative strategies. Additional propellant for orbit insertion means a heavier spacecraft at launch. Reducing or eliminating the need for propulsive maneuvers is essential to minimize cost. Aeroassist, which is the use of atmospheric forces to improve mission performance, is a proven technique and one that figures prominently in future missions.[1] The Mars Global Surveyor (Fig. 1) used aerobraking to reduce propulsive costs by 1200 m/s (about 380 kg of propellant) to reduce the orbit period from 48 h to 2 h (eccentricity from 0.9 to 0.1).[2–6] Similar aeroassisted techniques in the literature also provide reduction in propulsive maneuvers.[7–9]

Aerobraking methods as currently practiced have several disadvantages. Continuous ground observations of the spacecraft are required to control the orbital decay process safely. Communication is subject to a round-trip time delay, which is a significant fraction of the orbit period during the final stages of aerobraking. For example, a 40-min communications lag (the worst case at Mars) is severe for a 2-h orbit (a typical final orbit at Mars). Furthermore, aerobraking requires propulsive maneuvers after each drag pass to dump accumulated angular momentum. Although this dump maneuver typically requires only a few grams of propellant per orbit, the aerobraking phase can last for over 1000 orbits. In future missions demand for Deep Space Network links might outstrip availability making current (nonautonomous) aerobraking practices difficult.[10]

Lyons provides an overview of aerobraking automation options,[10] Hanna and Tolson provide accelerometer-based prediction of periapsis flythrough,[11] and Jah provides techniques for onboard navigation.[12] In this paper we consider several reaction-wheel control laws for a single-axis model, which automatically dump angular momentum (about the pitch axis) during atmospheric flythrough.

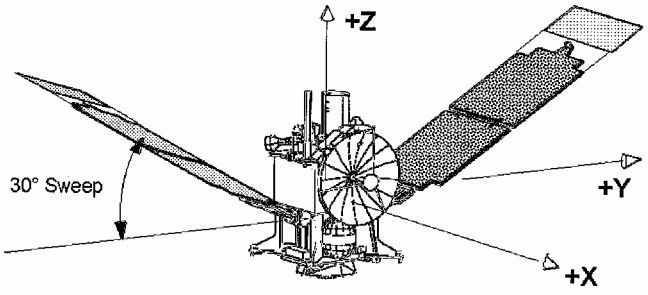

Fig. 1 Mars Global Surveyor spacecraft.

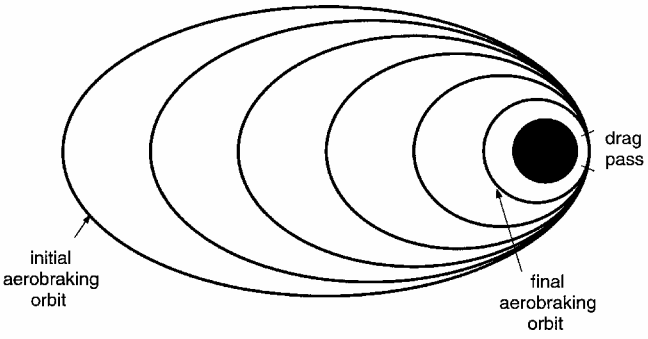

Fig. 2 Orbit decay during aerobraking.

We consider large off-nominal variations in atmospheric density for both large- and small-period orbits and evaluate the behavior of each control law. These reaction-wheel control laws can provide practical solutions to the problem of atmospheric timing error and to the larger problem of autonomous aerobraking.

Problem Description

Figure 2 illustrates how a spacecraft's orbit decays using aerobraking. The aerobraking phase begins in a high-energy orbit. During each pass, drag slows the spacecraft down, and the next orbit is smaller than the one before.[13]

Unfortunately, during the flythrough the spacecraft's attitude "weathervanes" about its two aerodynamically stable axes (pitch and yaw) as it flies through the atmospheric pass. When the spacecraft exits the atmosphere, it continues to rotate. On prior aerobraking missions propellant was needed to stop this rotation.

We devise a reaction-wheel control law for the pitch axis that meets several guidelines in order to support autonomous aerobraking. First and foremost, the control law must allow for a large timing margin for sequencing. The major contributions to timing errors are the uncertainty in the atmospheric density and in the orbit period. Next, the control law should be able to manage the total system angular momentum (i.e., by dumping it) so that propulsive desaturation of the reaction wheels is no longer needed. The control law should also require minimum instrumentation to avoid using expensive hardware. This guideline would also tend to make the controller easier to install on other spacecraft. We assume that the only state information available are the spacecraft and reaction-wheel spin rates. We also assume that the reaction wheels are small (i.e., they produce much smaller torques than that generated from the atmosphere). Finally, the control law should be simple to implement and to test.

In our scenario the reaction wheels absorb the angular momentum gained during the flythrough so as to negate the momentum already accumulated by the spacecraft. Because the aerodynamic torque is much stronger than the reaction-wheel torque, the pitch controller is unable to overcome weathervaning oscillations, but it can provide some damping—and it is able to dump angular momentum. By the end of the drag pass, the net total angular momentum is close to zero. Our approach uses only electrical power, which is replenished by the solar panel, thus saving precious propellant. After exiting the atmosphere, the spacecraft uses the reaction wheels to slew into position to communicate with Earth. Then, the spacecraft is given an inertial-attitude-hold command at the predicted attitude for zero entry angle of attack for the next flythrough, and the process repeats. In the following analysis we only consider rotation about the pitch axis. We expect yaw-axis behavior to be similar to that of the pitch axis. The roll axis is aerodynamically unstable but could be stabilized by using propellant or by articulating the solar panels. In either case the roll-axis dynamics do not contribute to the atmospheric timing margin.

Equations of Motion

Orbital

For three-dimensional gliding flight with lift and bank, about a nonrotating planet, the equations of motion are[13]

$$\dot{r} = V \sin\gamma \tag{1}$$

$$\dot{V} = \frac{-D}{m} - g \sin\gamma \tag{2}$$

$$V\dot{\gamma} = \frac{L\cos\sigma}{m} - g\cos\gamma + \frac{V^2\cos\gamma}{r} \tag{3}$$

$$\dot{\theta} = \frac{V\cos\gamma\cos\psi}{r\cos\phi} \tag{4}$$

$$\dot{\phi} = \frac{V\cos\gamma\sin\psi}{r} \tag{5}$$

$$V\dot{\psi} = \frac{L\sin\sigma}{m\cos\gamma} - \frac{V^2\cos\gamma\cos\psi\tan\phi}{r} \tag{6}$$

In this study we make a few idealized modeling assumptions. Aerobraking spacecraft [such as the Mars Global Surveyor (MGS)] tend to be symmetric and operate in the free-molecular flow regime. Thus, the instantaneous lift is very small, whereas the average lift is zero. (No lift effects were observed on the MGS mission.) Thus, we assume that the lift coefficient C_L is zero. Furthermore, we use a point–mass gravity field ($g = \mu/r^2$). Finally, we assume the spacecraft's orbit is planar ($\phi = \psi = 0$), and the atmosphere is exponential:

$$\rho = \rho_0 \exp[-\beta(r - r_0)] \tag{7}$$

where the model parameters are given in Table 1.

Attitude

Figure 3 depicts the position and velocity of the spacecraft. The angle of attack α is defined as the angle between the spacecraft

Table 1 Mars atmosphere parameters

Parameter	Reference value
ρ_0	55 kg/km^3
r_0	3507 km
β	0.145 km^{-1}

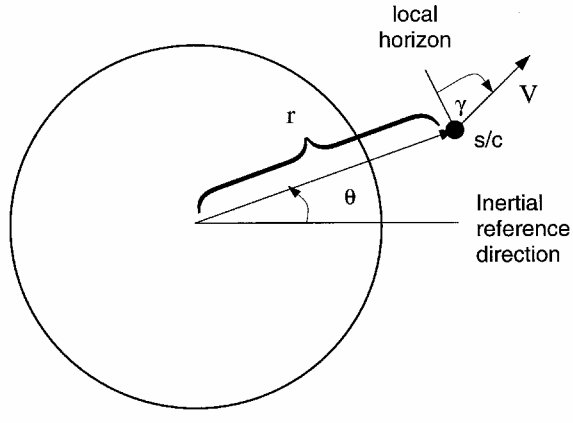

Fig. 3 Orbital position of spacecraft (r, θ) and velocity magnitude and flight-path angle (V, γ).

velocity vector and the body $-Z$ axis. We can calculate the inertial spin rate of the spacecraft as

$$\omega = \dot{\theta} - \dot{\gamma} + \dot{\alpha} \tag{8}$$

By substituting Eqs. (3) and (4) into Eq. (8), we find the equation of motion for the angle of attack α:

$$\dot{\alpha} = \omega - \frac{\mu \cos\gamma}{r^2 V} \tag{9}$$

The angular momentum of the spacecraft along the axis of rotation is

$$H_{\text{sc}} = I_{\text{sc}}\omega \tag{10}$$

The spacecraft has two torques along the axis of rotation: the external atmospheric torque and the internal reaction-wheel control torque. By differentiating Eq. (10) with respect to time and using Euler's law, we have

$$\dot{H}_{\text{sc}} = M \tag{11}$$

$$I_{\text{sc}}\dot{\omega} = \tfrac{1}{2}\rho V^2 A_{\text{ref}} L_{\text{ref}} C_{M_\alpha}\alpha - u \tag{12}$$

The (frictionless) reaction wheel only has one external torque acting on it: the control torque from the dc motor. This torque is identical in magnitude, but opposite in direction from the torque used for the spacecraft. Thus, the governing equation for the reaction wheel is

$$I_{\text{rw}}\dot{\Omega} = u \tag{13}$$

In summary, the attitude equations of motion are

$$\dot{\alpha} = \omega - \frac{\mu \cos\gamma}{r^2 V} \tag{14}$$

$$\dot{\omega} = \frac{\rho V^2 A_{\text{ref}} L_{\text{ref}} C_{M_\alpha}}{2I_{sc}}\alpha - \frac{u}{I_{\text{sc}}} \tag{15}$$

$$\dot{\Omega} = \frac{u}{I_{\text{rw}}} \tag{16}$$

Reaction-Wheel Control Laws

Inertial-Attitude-Hold Controller

In normal spacecraft operation the spacecraft is held in an inertially fixed attitude to either conduct science experiments or communicate with Earth. In our scheme we also have the spacecraft hold an inertially fixed attitude prior to atmospheric entry so that the angle of attack at entry is approximately zero. When the spacecraft does enter the atmosphere, no aerodynamic torques are present at first because the spacecraft is at a zero angle of attack. But as the spacecraft descends toward periapsis, the angle of attack decreases (to negative values), and the total system angular momentum changes as it is subjected to a growing external torque. The angle of attack decreases as a result of the natural motion of a nonrotating spacecraft to remain inertially fixed [which is also apparent in Eq. (14) for $\omega = 0$ and $\gamma \approx 0$]. Because the reaction wheels are commanded to maintain an inertial attitude, the change in momentum is transferred to the reaction wheels. Thus, the spacecraft senses atmospheric entry when the commanded torque u (or equivalently, the instantaneous change in total system angular momentum) exceeds some threshold. After this threshold is exceeded, the reaction wheel switches modes to an atmospheric control mode.

A risk in this type of threshold is the possibility that it will never be reached: the spacecraft can stay in an inertial attitude for an entire drag pass without ever activating the atmospheric control mode. Fortunately, this is almost never the case. Because the angle of attack starts at nearly zero and decreases monotonically after that, the torque magnitude u will increase monotonically, causing the threshold to eventually be met. In simulations we find that the atmospheric control law is not triggered when the trigger threshold is 100% of the maximum available reaction-wheel torque and the dynamic pressure at periapsis is less than 10% of the nominal case. For a more reasonable trigger threshold of 5%, the atmospheric density must be 0.5% nominal (a -3.3σ variation) or less to not trigger the control law. However, when the control fails to trigger in the 5% threshold case no harm is done: the atmospheric density is too low to change the spacecraft's velocity or angular momentum.

Once atmospheric entry is detected, and the reaction wheel switches to atmospheric control mode, an onboard timer is started. The timer counts down the time until the spacecraft is predicted to exit the atmosphere, at which point the reaction wheels will once again switch modes—this time, back to the inertial-attitude-hold mode. This timed event can be calculated a priori by simulations of a nominal atmospheric flythrough.

Spin-Down Controller

We introduce a simple control law that despins the reaction wheel during the atmospheric flythrough. Upon reaching zero-spin rate, the applied reaction-wheel torque is shut off. After exiting the atmosphere, all residual spacecraft momentum is transferred back to the reaction wheel.

During the flythrough, the spacecraft can torque against the atmosphere. The atmosphere tends to keep the spacecraft in place (oscillating about an average angle of attack near zero) while the wheel is desaturated. Ideally, the spin-down control law is activated at periapsis, where the atmosphere is densest. For a given orbit the time between atmospheric entry and periapsis passage can be computed a priori for the nominal atmosphere. In this ideal case the reaction wheels begin to spin down at periapsis. If the density is off nominal, the spin-down law will be activated a little before or after periapsis. The effect of these timing errors is most detrimental in high-period orbits, when the drag pass is short in duration.

This control law has the advantage of being exceedingly simple to implement and being independent of spacecraft and planetary parameters. However, it turns out to be the least robust of our proposed controllers.

Affine Partial-State Controller

With the exception of the second term of Eq. (14), Eqs. (14–16) describe a system of linear equations, where we are considering the dynamic pressure term, $\rho V^2/2$ to be a time-varying parameter. To simplify our analysis, we approximate the term $\mu \cos\gamma / r^2 V$ with a constant, its value at periapsis. We can now rewrite Eqs. (14–16) as

$$\dot{\boldsymbol{x}} = A(t)\boldsymbol{x} + Bu + E \tag{17}$$

where

$$\boldsymbol{x} = [\alpha \quad \omega \quad \Omega]^T \tag{18}$$

$$A(t) = \begin{bmatrix} 0 & 1 & 0 \\ -a(t) & 0 & 0 \\ 0 & 0 & 0 \end{bmatrix} \tag{19}$$

$$B = \begin{bmatrix} 0 & -I_{\text{sc}}^{-1} & I_{\text{rw}}^{-1} \end{bmatrix}^T \tag{20}$$

$$E = \begin{bmatrix} -\mu/r_p^2 V_p & 0 & 0 \end{bmatrix}^T \tag{21}$$

where $a(t) = -\rho V^2 A_{\text{ref}} L_{\text{ref}} C_{M_\alpha}/2I_{sc}$.

The output we are interested in is H_{total}, the total system angular momentum, which we wish to drive to zero. We observe that $H_{\text{total}} = C\boldsymbol{x}$, where

$$C = [0 \quad I_{\text{sc}} \quad I_{\text{rw}}] \tag{22}$$

We can further simplify the analysis by assuming $a(t) \approx a_p$. In this final form we have a set of affine time-invariant differential equations. This form is equivalent to a linearized system (with the same A, B, and C matrices) where the state vector $\boldsymbol{x}$ would be redefined by subtracting off its equilibrium value $\boldsymbol{x}_e$. This equilibrium state is computed by solving Eqs. (14–16) for $\dot{\alpha} = \dot{\omega} = \dot{\Omega} = u = 0$. This process yields

$$\omega_e = \mu / r_p^2 V_p \tag{23}$$

$$\alpha_e = 0 \tag{24}$$

For the total momentum to be driven to zero, we have

$$H_{\text{total},e} = I_{\text{sc}}\omega_e + I_{\text{rw}}\Omega_e \tag{25}$$

$$0 = I_{\text{sc}}\omega_e + I_{\text{rw}}\Omega_e \tag{26}$$

$$\Omega_e = \frac{-I_{\text{sc}}\omega_e}{I_{\text{rw}}} \tag{27}$$

$$= \frac{-I_{\text{sc}}\mu}{I_{\text{rw}} r_p^2 V_p} \tag{28}$$

Thus,

$$\boldsymbol{x}_e = \left(\mu / r_p^2 V_p\right)[0 \quad 1 \quad -I_{\text{sc}}/I_{\text{rw}}]^T \tag{29}$$

If the system (A, B, C) can be stabilized with an appropriate control u, then our system angular momentum H will be asymptotically driven to zero. To convert the affine system into a linear system using state feedback, we require that $u = \boldsymbol{K}(\boldsymbol{x} - \boldsymbol{x}_e)$. A control feedback gain vector $\boldsymbol{K} = [K_\alpha \;\; K_\omega \;\; K_\Omega]^T$ is selected to stabilize the closed-loop system. Because this is a time-varying system, having eigenvalues of $A + B\boldsymbol{K}$ in the open left-half plane does not guarantee asymptotic stability. From a practical standpoint the state variables ω and Ω can be measured with a body-fixed gyro and reaction-wheel tachometer (where the inertial rate Ω is the sum of the body rate ω and the relative rate as measured by the tachometer). Unfortunately, the spacecraft does not have any instrumentation onboard to measure the state variable α. Thus, we add the constraint $K_\alpha = 0$ to our optimization problem.

We take a minimax approach, where we pick the gain vector $\boldsymbol{K}$ that minimizes the maximum real part of the eigenvalues of $A + B\boldsymbol{K}$. This minimax problem has an analytic solution[14]:

Table 2 Reference spacecraft parameters

Parameter	Reference value
Mass	1000 kg
C_D	2.0
C_{M_α}	$-0.00366\ \text{deg}^{-1}$
A_{ref}	$17.44\ \text{m}^2$
L_{ref}	8.73 m
Max reaction-wheel torque	$0.18\ \text{N}\cdot\text{m}$
Reaction-wheel capacity	$27.0\ \text{N}\cdot\text{m}\cdot\text{s}$
I	$1000\ \text{kg}\cdot\text{m}^2$
J	$0.0645\ \text{kg}\cdot\text{m}^2$

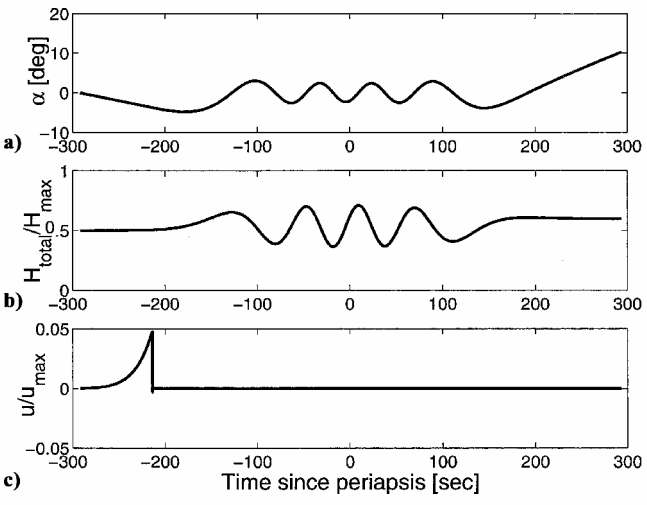

Fig. 4 Sample time history during a single flythrough for no atmospheric control (i.e., $u = 0$): a) angle of attack α, b) total system momentum $H_{\text{total}}/H_{\text{max}}$, and c) commanded reaction-wheel torque u/u_{max}.

$$K_\omega = 8I\sqrt{3a_p}/9 \tag{30}$$

$$K_\Omega = -\left(J\sqrt{3a_p}/9\right) \tag{31}$$

Numerical simulations demonstrate stable behavior.

The equilibrium value x_e is a function of the orbit. Two independent parameters are needed to specify the orbit size and shape. We use the dynamic pressure at periapsis as one of these, which we set to $0.5\ \text{N/m}^2$ for the nominal case (a typical heating constraint on prior aerobraking missions[4]). The remaining parameter can be dealt with in two ways. The first method is to use the orbit period (which the spacecraft can roughly measure by timing the interval between successive drag passes) and then use a look-up table on each orbit to ascertain the optimum $\boldsymbol{K}$. The second is to design a fixed $\boldsymbol{K}$ to be used for all drag passes using the "average" aerobraking orbit as the specification (e.g., we assume the orbit eccentricity is 0.4). The second approach is simpler to implement and yields results only slightly worse than the first approach.

The resulting affine partial-state control law stabilizes the system, even though the angle of attack cannot be measured. Simulations show that an affine full-state control law yields superior performance. One idea for implementing the full-state feedback controller is to use a state observer to estimate α. Unfortunately, applying the minimax approach to an observer does not work with this time-varying system because the state estimate of α turns out to be unstable.

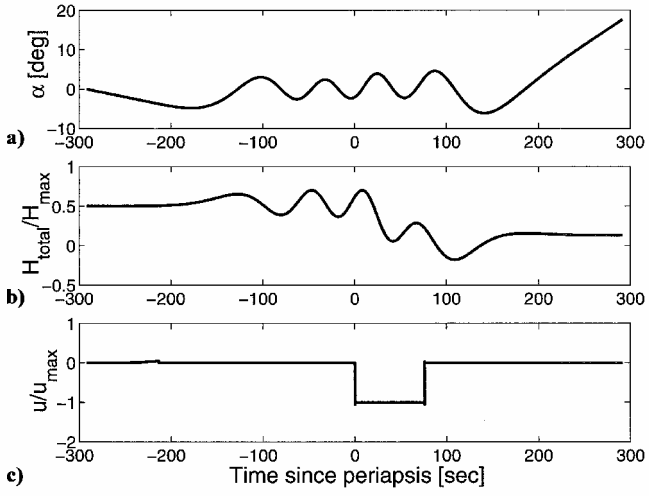

Fig. 5 Time history for the spin-down controller: a) angle of attack α, b) total system momentum $H_{\text{total}}/H_{\text{max}}$, and c) commanded reaction-wheel torque u/u_{max}.

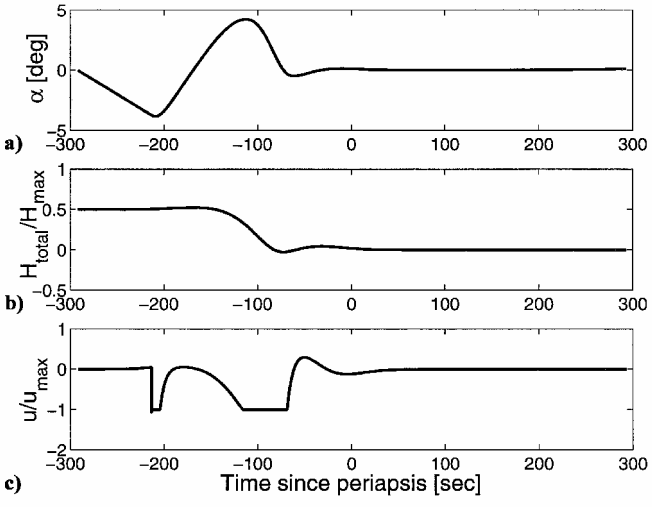

Fig. 6 Time history for the affine partial-state controller: a) angle of attack α, b) total system momentum $H_{\text{total}}/H_{\text{max}}$, and c) commanded reaction-wheel torque u/u_{max}.

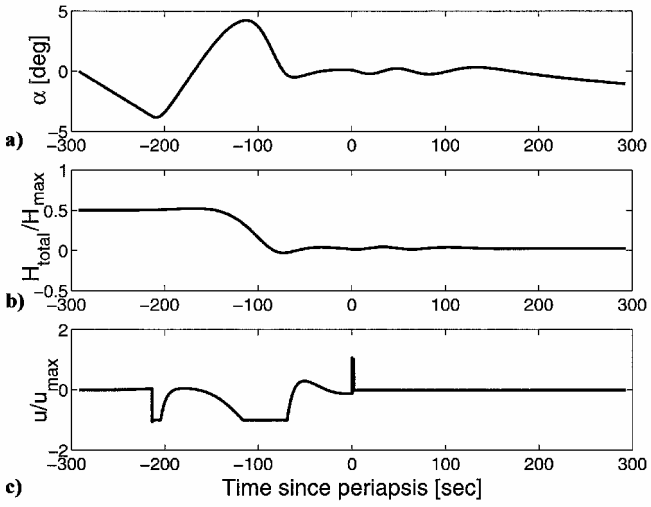

Fig. 7 Time history for the two-stage controller: a) angle of attack α, b) total system momentum $H_{\text{total}}/H_{\max}$, and c) commanded reaction-wheel torque $u/u_{\max}$.

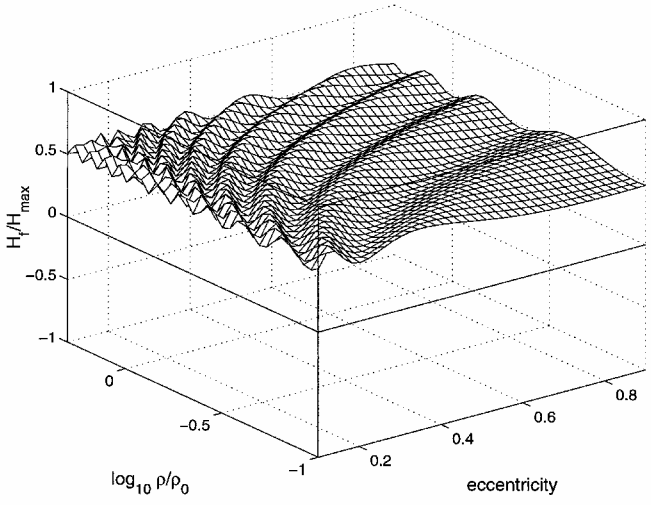

Fig. 8 Final momentum of the spacecraft using no atmospheric control as a function of eccentricity and atmospheric density. The initial momentum for this case is 50% of the reaction-wheel maximum.

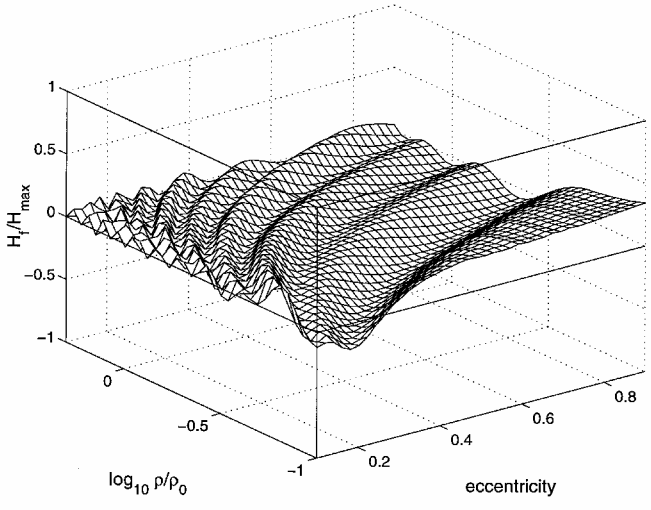

Fig. 9 Final momentum of the spacecraft using the spin-down controller.

Two-Stage Controller

In simulations the affine partial-state control law tends to damp out oscillations rapidly in angle of attack. Under ideal conditions the spacecraft's attitude reaches its equilibrium state before periapsis. But for low atmospheric density and high-orbit-period cases, the affine partial-state controller can take longer to stabilize than the flythrough time. We note that the affine partial-state controller tends to do most (if not all) of its work before periapsis, whereas the spin-down controller does all of its work after periapsis. We thus combine the two control laws into a "two-stage" controller, with the expectation that it will be more robust than the other two.

No Control

Let us consider the case of no control, where the attitude-hold mode of the reaction wheel is turned off once the atmosphere is detected. That is, let $u = 0$. Following the linearization procedure just outlined (and examining just the attitude and attitude-rate state variables), we have the linearized system

$$\dot{\boldsymbol{x}} = A(\boldsymbol{x} - \boldsymbol{x}_e) \tag{32}$$

where

$$\boldsymbol{x} = [\alpha \quad \omega]^T \tag{33}$$

$$A(t) = \begin{bmatrix} 0 & 1 \\ -a(t) & 0 \end{bmatrix} \tag{34}$$

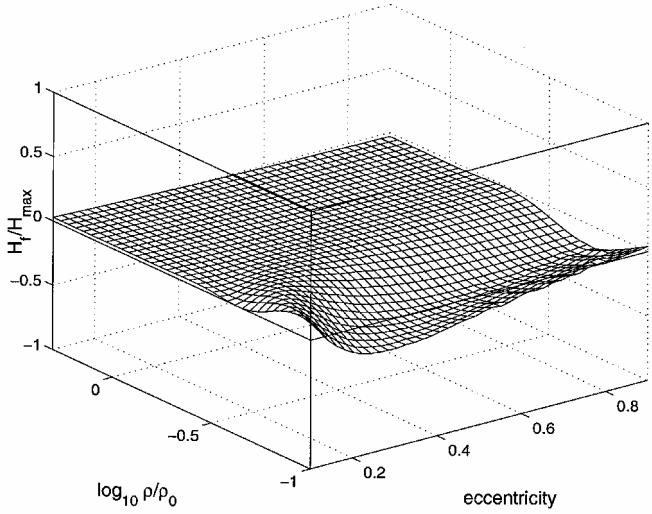

Fig. 10 Final momentum of the spacecraft using the affine partial-state controller.

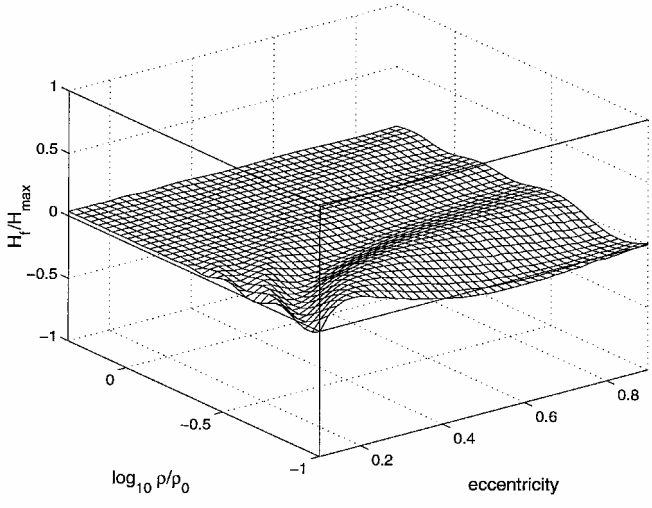

Fig. 11 Final momentum of the spacecraft using the two-stage controller.

$$\boldsymbol{x}_e = \begin{bmatrix} 0 & -\mu/r_p^2 V_p \end{bmatrix}^T \tag{35}$$

The eigenvalues of this system are on the imaginary axis, and thus the system is undamped. The angle of attack will tend to oscillate with a fixed amplitude. The ΔH incurred on such a drag pass will depend on the relative phasing of α with the dynamic pressure. Each half-oscillation will cause momentum to be gained or lost. The net gain after the drag pass will depend on the initial conditions of the pass. But because of the natural revolution of the spacecraft around the planet, the average angle of attack is biased (toward negative values). Most uncontrolled orbits will result in a net gain of angular momentum, whereas some will result in a net loss of angular momentum. Thus, on average the angular momentum will tend to grow over the course of many atmospheric flythroughs.

Results

In general, the performance of a controller during an atmospheric drag pass depends on a number of parameters: the orbit period, periapsis altitude, atmospheric density, initial angular momentum, and the atmospheric trigger threshold. We target the periapsis altitude so that the dynamic pressure is 0.5 N/m.^{2} (We assume the atmospheric density is nominal, which may not be the case.) We also set the trigger threshold to 5%, which yields the best results in our simulations. There are still too many remaining "free" parameters to be able to examine the entire simulation space. Instead, we examine some representative cases and some cross sections of the solution space. Dispersions in parameters included in $a(t)$ (A_{ref}, L_{ref}, C_{M_α}, I_{sc}) will tend to have the same effect as a dispersion in the atmospheric density.

Simulation Methods

We use an RK45 method with a relative tolerance of 10^{-7} to integrate the equations of motion. The controller output is sampled at each integration timestep. The controller would typically run at a sampling rate of 10 ms. The Nyquist rate for the controller sampling rate is thus 20 ms (or 50 Hz). As seen in the time histories (Figs. 4–7), this sampling rate is more than sufficient to keep up with the governing dynamics (i.e., there are no high-frequency components in the control). Table 2 presents the reference spacecraft parameters used in the simulations.

Single Drag Pass

Figures 4–7 present sample time histories for each of our controllers. The initial reaction-wheel momentum in all cases is 50% of capacity. The applied torque, until about 200 s before periapsis, is the torque required to maintain an inertial attitude. Afterward, the atmospheric controller is triggered.

In the no-control case (Fig. 4) the natural oscillatory motion of the angle of attack is apparent. This motion causes the total system momentum to oscillate as well. The final momentum is a function of the peak amplitude of α and the value of α at periapsis. For the net change in angular momentum to be zero, any momentum gained before periapsis needs to be lost after periapsis. A zero net change is only possible when the angle of attack is an odd function

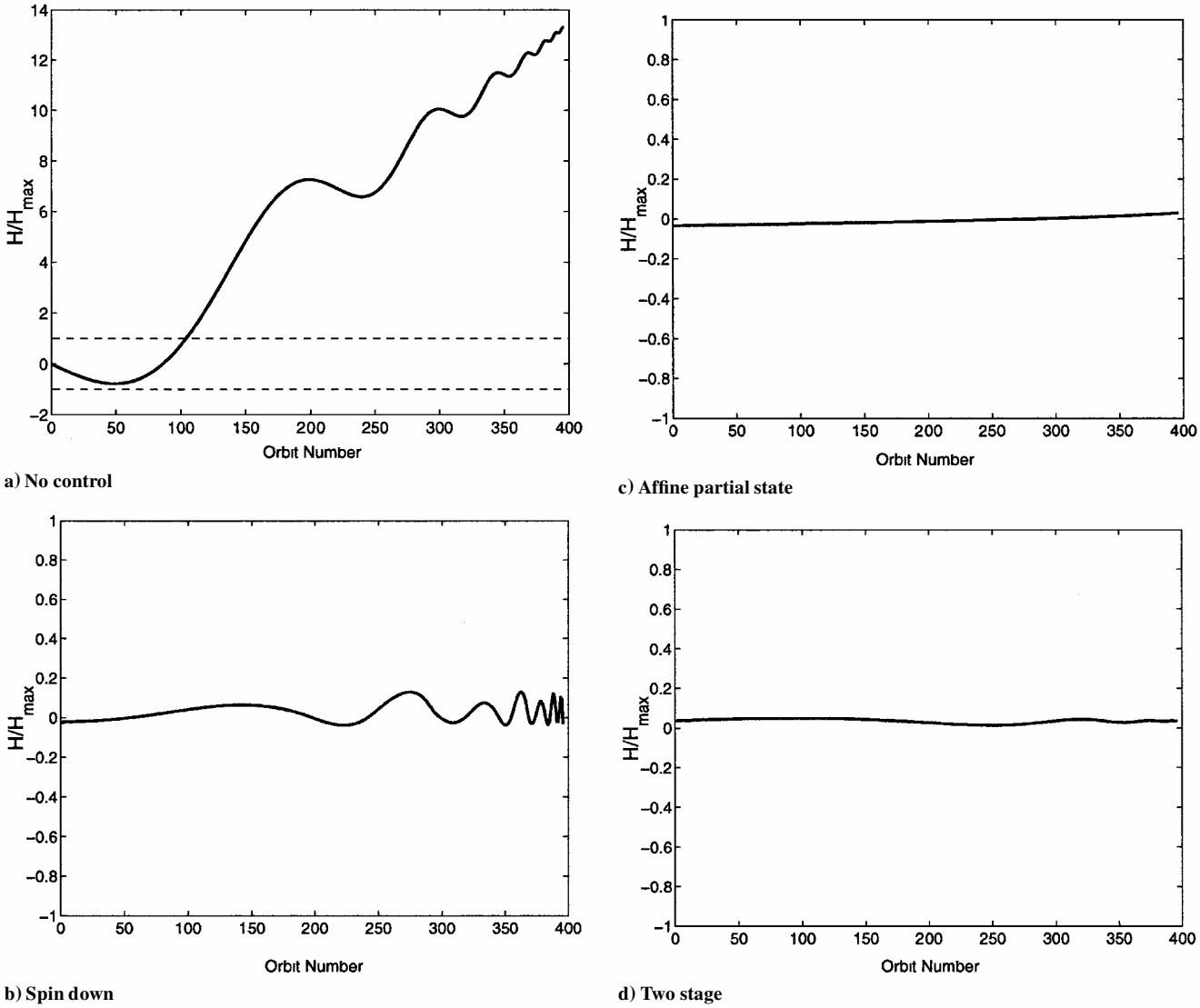

Fig. 12 Normalized total system angular momentum after consecutive drag passes. The initial orbit period is 48 h, and the final orbit period is 2 h. The atmospheric density is assumed to be nominal.

$[\alpha(t-t_p) = -\alpha(t_p - t)]$. The timing with respect to periapsis is important because the density profile is approximately an even function $[\rho(t-t_p) \approx \rho(t_p - t)]$. When the value of α at periapsis is zero, the gain in angular momentum is nearly zero.

The spin-down controller (Fig. 5) performs somewhat better than the no-control case. At periapsis the spacecraft begins its momentum dump. This controller is not able to damp the angle-of-attack oscillations and thus acquires some residual angular momentum by the end of the drag pass. However, this controller is able to dump its initial momentum and thus does not tend to accumulate momentum over repeated drag passes. In the special case where the initial momentum is zero, this controller is identical to the no-control case because there is no momentum to dump.

The affine partial-state controller (Fig. 6) almost immediately drives the momentum to zero. By periapsis the angle of attack is driven to nearly zero.

The two-stage controller (Fig. 7) exhibits features similar to the preceding two. In this case the momentum dump at periapsis is detrimental because angle-of-attack oscillations continue (but at a significantly reduced amplitude), and thus the total system momentum slightly increases. As mentioned earlier, the two-stage controller is more effective than the affine partial-state controller in thin atmospheric conditions.

The time histories of Figs. 4–7 are valid for only one set of initial conditions. To get a better idea of the overall performance, we simulate each controller over a range of orbit sizes and density fluctuations. These results are shown in Figs. 8–11. Each point on the surface plot represents a single drag pass for a given eccentricity and periapsis density. Uncertainty in atmospheric densities at periapsis ranges from 10% nominal (−1 on the log scale) to 200% nominal (0.3 on the log scale). Nominal density is zero on the log scale.

In the no-control case (Fig. 8) the initial bias of 50% capacity remains in the final momentum. Again, the fluctuations are merely a geometric representation of the amplitude and phase of the angle-of-attack oscillations. The same rippling effect is present in the spin-down case (Fig. 9). The spin-down controller removes the initial bias (except in the low-density, high-eccentricity case, where the remaining flythrough time after triggering is too short) but still has residual angular momentum after the flythrough. The affine partial-state controller (Fig. 10) is flat for most cases. As already noted, this controller must be configured for a specific eccentricity. In this case that eccentricity is 0.4, which roughly marks the halfway point of a typical aerobraking phase. Because of the discrepancy between the actual orbit size and the assumed orbit size, Fig. 10 has a gentle downward slope, as density decreases. In a similar manner to the spin-down controller, when the density is very low and the orbit period high, the flythrough time is short, and thus this controller runs out of time before it is able to reach equilibrium.

To address the problem of short flythrough times, the two-stage controller (Fig. 11) switches from the partial-state law to

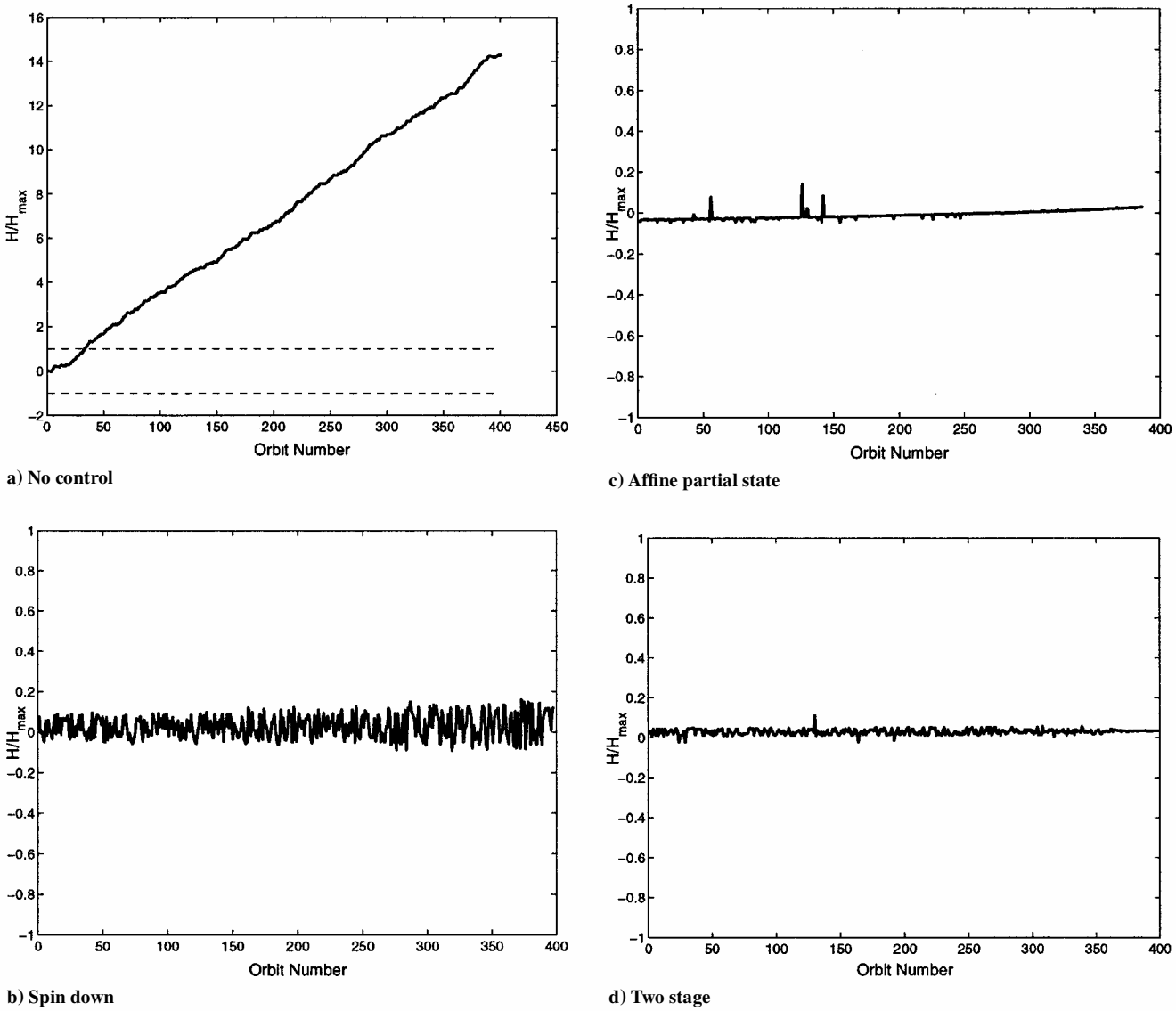

Fig. 13 Normalized total system angular momentum after consecutive drag passes. The atmospheric density is assumed to be Gaussian, with $\sigma = 30\%$.

the spin-down law at the estimated time of periapsis passage. This switch results in a much flatter plot overall, which indicates the final momentum is consistently closer to zero.

Multiple Drag Passes

A control law that performs well on one drag pass might not necessarily perform well on repeated drag passes. We thus simulate an entire aerobraking mission, starting at a 48-h orbit and terminating when a 2-h orbit is achieved. Figure 12 depicts the total system momentum history as a function of orbit number for a nominal atmosphere.

The no-control case has a positive bias in the change in angular momentum, as expected from our analysis of the equations of motion. We note that after only a few orbits the total angular momentum exceeds the reaction wheel's capacity (by 1200%). Propulsive momentum dumping would therefore have to be repeatedly used to offset this bias.

The spin-down case is similar to the no-control case, but with the secular term (i.e., the bias) removed. Because the spin-down law is capable of keeping the momentum well within the physical limits of the reaction wheel, this law is feasible.

The affine partial-state law works very well. The eccentricity bias is clearly visible in Fig. 12c, where the angular momentum becomes zero at about orbit 200, which corresponds to an eccentricity of 0.4.

Unfortunately, the Martian atmosphere is highly variable, with a 1-σ atmospheric density variation of about 30%. Figure 13 illustrates a multiple drag pass analysis, which takes density variations into account. The atmospheric densities are assumed independent from pass to pass. In this random-atmosphere case the no-control case is still unbounded. The spin-down law has a much noisier momentum history. The affine partial-state law has a response very similar to the nominal case, but with a few spikes coinciding with the low-density passes. Finally, the two-stage controller is noisier than affine partial-state controller, but with a lower peak deviation.

Momentum Gain Analysis

We now consider the effect of random initial momentum. Up until now, the initial momentum for each drag pass has either been arbitrarily set to 50% of reaction-wheel capacity (for the single-pass case) or set to the final momentum of the previous pass (for the multiple pass case).

In this analysis we simulate thousands of drag passes for 19 specific atmospheric densities (ranging from 10 to 200% of the nominal case) for random orbit sizes and random initial momenta. Eccentricities are selected from a uniform distribution, ranging from 0.1 to 0.9. Initial momenta are assumed Gaussian, with zero mean and a standard deviation of 25% reaction-wheel capacity. We then calculate the gain as the standard deviation of the postflyby momenta, normalized by the standard deviation of the preflyby momenta. We also calculate the resulting bias as the mean postflyby momenta, normalized by the standard deviation of the preflyby momenta. We will refer to these two quantities as the gain G and the bias B given by

$$G = \frac{\sigma(H_f)}{\sigma(H_i)} \tag{36}$$

$$B = \frac{\mathrm{Avg}(H_f)}{\sigma(H_i)} \tag{37}$$

The square of G represents the transfer function gain from the preflyby momenta to the postflyby momenta. A nonzero value of B indicates a bias in the final momentum. The normalized gain and bias are shown in Fig. 14.

For densities greater than 20% nominal, the affine partial state performs better than the spin-down controller. In all cases the two-stage controller has the smallest gain. For most densities the affine partial-state controller has the smallest bias. Finally, the no-control case is the only one that has a gain greater than one, indicating instability.

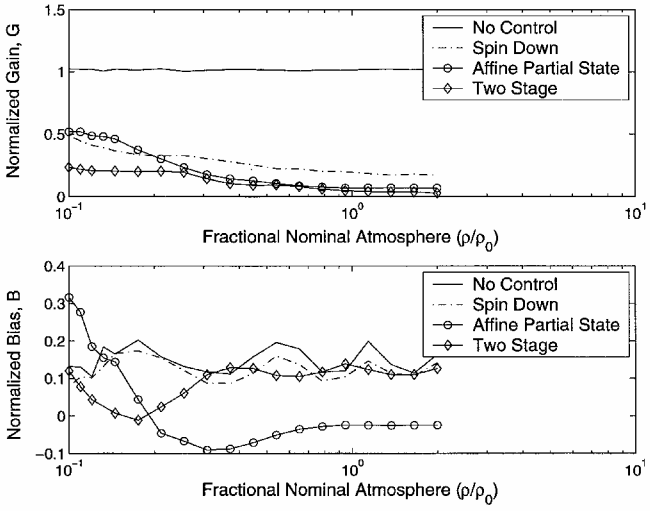

Fig. 14 Normalized gain G and the normalized bias B for each controller as a function of atmospheric density.

Conclusions

A reaction-wheel controller can provide robust control during atmospheric drag passes while providing a free desaturation of stored angular momentum. In this paper three reaction-wheel controllers are compared: spin down, affine partial state, and two stage. Each of these controllers enables the timing margin for sequencing to be increased significantly, making autonomous aerobraking more robust. A larger timing margin can even enable autonomous aerobraking at moderately large orbit periods for spacecraft that do not carry an accelerometer.

Of the proposed control laws the spin-down controller is the simplest. This controller is spacecraft independent and works equally well in thick or thin atmospheres. The affine partial-state controller is more complex than the spin-down, while still only relying on readily available angular rate information. This controller is much better at dumping momentum in moderate to thick atmospheres and still works in thin atmospheres. The two-stage controller enjoys the advantages of both the spin-down and affine partial-state controllers. All of these controllers can achieve robust attitude control in the environment of large atmospheric density and timing uncertainties.

Acknowledgments

This work was funded in part by the Jet Propulsion Laboratory, California Institute of Technology, Pasadena, California, under JPL Contract 1223406 (G. T. Rosalia, Contract Manager, and Dennis V. Byrnes, Technical Manager). Portions of this work described were performed at the Jet Propulsion Laboratory, California Institute of Technology, under contract with NASA.

References

[1]Braun, R. D., "Aeroassist Systems: An Important Element in NASA's New Era of Planetary Exploration," *Journal of Spacecraft and Rockets*, Vol. 36, No. 3, 1999, p. 297.

[2]Munk, M., and Powell, R., "Aeroassist Technology Planning for Exploration," *Advances in the Astronautical Sciences*, Vol. 105, Pt. 2, 2000, pp. 1073–1083.

[3]Spencer, D., and Braun, R., "Mars Pathfinder Atmospheric Entry: Trajectory Design and Dispersion Analysis," *Journal of Spacecraft and Rockets*, Vol. 33, No. 5, 1996, pp. 670–676.

[4]Lyons, D., "Aerobraking at Venus and Mars, a Comparison of the Magellan and Mars Global Surveyor Aerobraking Phases," American Astronautical Society, AAS Paper 99-358, Aug. 1999.

[5]Lyons, D., Beerer, J., Esposito, P., Johnston, M., and Willcockson, W., "Mars Global Surveyor: Aerobraking Mission Overview," *Journal of Spacecraft and Rockets*, Vol. 36, No. 3, 1999, pp. 307–313.

[6]Wilmoth, R. G., Rault, D. F., Cheatwood, F. M., Engelund, W. C., and Shane, R. W., "Rarefied Aerothermodynamic Predictions for Mars Global Surveyor," *Journal of Spacecraft and Rockets*, Vol. 36, No. 3, 1999, pp. 314–322.

[7]Lyons, D., "Aerobraking Magellan: Plan Versus Reality," *Advances in the Astronautical Sciences*, Vol. 87, Pt. 2, Feb. 1994, pp. 663–680.

[8]Tragesser, S., and Longuski, J., "Analysis and Design of Aerocapture Tether with Accounting for Stochastic Errors," *Journal of Spacecraft and Rockets*, Vol. 35, No. 5, 1998, pp. 683–689.

[9]Longuski, J., Puig-Suari, J., and Mechalas, J., "Aerobraking Tethers for the Exploration of the Solar System," *Acta Astronautica*, Vol. 35, No. 2/3, 1995, pp. 205–214.

[10]Lyons, D., "Aerobraking Automation Options," American Astronautical Society, AAS Paper 01-385, Aug. 2001.

[11]Hanna, J., and Tolson, R., "An Approach for Autonomous Aerobraking to Mars," American Astronautical Society, AAS Paper 01-387, Aug. 2001.

[12]Jah, M., "Accelerometer Data as an Observation Type for Mars Aerobraking Missions: Phase A Study," American Astronautical Society, AAS Paper 01-386, Aug. 2001.

[13]Vinh, N., Busemann, A., and Culp, R., *Hypersonic and Planetary Entry Flight Mechanics* Univ. of Michigan Press, Ann Arbor, MI, 1980, Chaps. 1 and 2.

[14]Johnson, W., "Analysis and Design of Interplanetary Aeroassisted Missions," Ph.D. Dissertation, School of Aeronautics and Astronautics, Purdue Univ., West Lafayette, IN, Dec. 2002.

C. A. Kluever
Associate Editor